

SPECTRAL EMISSIONS AND DOSIMETRY OF METAL TRITIDE PARTICULATES

D. J. Strom, R. D. Stewart, and J. C. McDonald
Pacific Northwest National Laboratory Richland
Washington 99352, USA

Received October 4 2001, amended January 2 2002, accepted January 11 2002

Abstract — Inference of intakes and doses from inhalation of metal tritide particles has come under scrutiny because of decommissioning and decontamination of US Department of Energy facilities. Since self-absorption of radiation is very significant for larger particles, interpretation of counting results of metal tritide particles by liquid scintillation requires information about emission spectra. Similarly, inference of dose requires knowledge of charged particle and photon spectra. The PENELOPE Monte Carlo radiation transport computer code was used to compute spectral emissions and other dosimetric quantities for tritide particulates of Sc, Ti, Zr, Er, and Hf. Emission fractions, radial absorbed dose distributions, specific energy distributions and related frequency-mean specific energies and lineal energies, and the emitted spectra of electrons and bremsstrahlung photons are presented for selected particulates with diameters ranging from about 0.01 μm to 25 μm . Results characterising the effects of uncertainties associated with the composition and density of the tritides are also presented. Emission spectra are used to illustrate trends in the relationship between 'apparent' and 'observed' activity as a function of particle type and size. Emissions from metal tritide particles are weakly penetrating, and electron emission spectra tend to 'harden' as particle size increases. Microdosimetric considerations suggest that the radiation emitted by metal tritides can be classified as a low linear energy transfer radiation source. For cells less than about 7 μm away from the surface of a metal tritide, the primary dose component is due to electrons. However, bremsstrahlung radiation may deposit some energy tens, hundreds or even thousands of micrometres away from the surface of a tritide particle. The data and analyses presented in this report will help improve the accuracy of dose determinations for particulates of five metal tritides. Future work on the spectral emissions and dosimetry of metal tritide particulates needs to consider the contributions of so-called internal bremsstrahlung, an additional form of bremsstrahlung radiation emitted during beta decay.

INTRODUCTION

Metal tritides such as scandium tritide (ScT_2), titanium tritide (TiT_2), zirconium tritide (ZrT_2), erbium tritide (ErT_2) and hafnium tritide (HfT_2) are sometimes encountered in the workplace and may present radiological protection problems resulting from their incorporation into the body through a number of pathways. The uptake and retention of tritium in the body depends upon its chemical form and the method of entry. When metal tritides are present as fine powders, inhalation may result in dose being delivered to lung tissue by the primary beta particles emitted by tritium or by the secondary bremsstrahlung radiation produced when electrons decelerate because of collisions inside the metal tritide or in the surrounding tissue medium. Dosimetry calculations for tritium provided by the International Commission on Radiological Protection publications mainly deal with tritium in the form of the elemental gas, tritiated water or organically bound tritium^(1–4). Some information on particulate tritides is provided in ICRP publications 71⁽⁴⁾ and 72⁽⁵⁾. Recently, additional information on metal tritide metabolism has become available^(6–9).

Metal tritides can present significant radiation protec-

tion problems if they are inhaled during work procedures, or because of an accident, and retained in the lung in a fashion similar to ICRP solubilisation class M (moderate rate) or S (slow rate) materials⁽¹⁰⁾. For some of the aforementioned compounds, the tritium is well retained and does not dissociate from the metal. Depending on the size of the particle and its composition, much of the tritium beta energy will not exit the particle. In addition, electron interactions with the metal tritide and surrounding tissue produce bremsstrahlung radiation that can deposit energy much farther away from the particle surface than the beta particles directly emitted by the tritium. For these reasons, the ICRP-tabulated dose coefficients for tritium need to be supplemented with additional calculations to improve the accuracy of dose evaluations for metal tritides.

Considering the relatively low energy of the radiation emitted from a metal tritide particle, which may be only a few micrometres in diameter, direct measurements of energy spectra are difficult or impossible. Mathematical simulations of the particles and the radiation fields surrounding them are possible using codes such as MCNP⁽¹¹⁾ or EGS-4⁽¹²⁾, but there are some limitations to the cross section data contained in both of these codes. For this work, a relatively new code has been used to evaluate both the beta particle and bremsstrahlung fluence spectra. Additional microdosimetric calculations have been performed to provide information for

the interpretation of biological effects produced by these radiations.

METHODS

Radiation transport

PENELOPE, an acronym for PENetration and Energy LOss of Positrons and Electrons, is a general purpose Monte Carlo code to simulate the behaviour of ionising electrons and photons in arbitrary materials composed of elements with atomic numbers from 1 to 92⁽¹³⁻¹⁵⁾. PENELOPE implements a so-called mixed simulation algorithm⁽¹³⁾ in which 'hard' electron and positron interactions are simulated in a detailed way while 'soft' interactions are calculated from multiple scattering theory⁽¹⁶⁾. For higher energy electrons and photons, benchmarking activities by Sempau *et al.*⁽¹⁵⁾ demonstrate that PENELOPE compares favorably to the EGS4⁽¹²⁾, ETRAN⁽¹⁷⁾, and ITS3⁽¹⁸⁾ Monte Carlo code systems. However, PENELOPE is capable of transporting electrons and positrons down to energies as low as 100 eV. To our knowledge, PENELOPE is the first general purpose Monte Carlo code capable of transporting electrons and positrons in arbitrary media down to such low-energies*. Condensed history Monte Carlo codes such as EGS4, ETRAN, ITS3, and MCNP⁽¹¹⁾ are generally limited to primary electron energies above about 1 to 20 keV.

The physics model and cross sections implemented in the PENELOPE code system have been described in detail by others⁽¹³⁻¹⁵⁾. The crucial component of the PENELOPE code system is a set of Fortran 77 routines that allow a user to perform 'near analog' electron-photon simulations with little prior knowledge of electron and photon transport physics. That is, the user supplies routines to record (or 'tally') the location of energy transfer events, control the overall evolution of particle tracks (e.g. creation of source particles), and determine the geometry of the materials used in the simulation. The intricacies of sampling from the relevant cross section tables and temporary storage of secondary particles created during the transport of a primary (source) particle are automatically and transparently handled within the PENELOPE transport kernel.

The Pacific Northwest National Laboratory (PNNL) has developed a custom application, called TPD (an abbreviation for tritide particle dosimetry), based on the standard PENELOPE physics and cross sections. The

TPD computer program calculates dosimetric and microdosimetric quantities for a spherical region of radioactive material (i.e. the source region) surrounded by an infinite medium of the same or a different material, and dosimetric and microdosimetric quantities are tallied in the regions indicated in Figure 1. The initial location of the primary electrons emitted by tritium is determined by random sampling from within the source region. For point sources, i.e. particles 0 μm in diameter, random sampling of the initial source particle location is turned off. In the present work, calculations are based on tritide particles embedded in an infinite medium of four-element International Commission on Radiation Units and Measurements (ICRU) soft tissue (1.0 g.cm^{-3})⁽¹⁴⁾.

Although event-by-event Monte Carlo codes such as OREC^(19,20) and PITS^(21,22) represent the preferred method of computing distributions of microdosimetric quantities, the cross sections needed to perform event-by-event simulations are usually only available for water. Moreover, Stewart *et al.*⁽²³⁾ showed that, for site sizes such as those considered in this article, PENELOPE-calculated site-hit probabilities, single-event distributions, and the frequency-mean specific energies are in reasonable agreement with those predicted using event-by-event Monte Carlo.

Several simulation-control parameters are used in PENELOPE to determine when the detailed (hard collision) physics model is used instead of multiple scattering theory. The selection of simulation-control parameters can affect the estimation dosimetric and, especially, microdosimetric quantities for small particle sizes and tally regions. For the results presented in this article, simulation-control parameters were selected to give a detailed treatment of electron elastic and inelastic collisions⁽²³⁾. Electrons and positrons with kinetic ener-

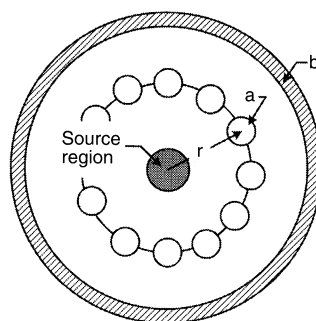


Figure 1. Schematic illustrating the annular tally regions and spherical sites used to tabulate dosimetric and microdosimetric quantities. (a) Microdosimetric quantities are tabulated in 10 spherical sites located distance r from the centre of the source region. Microdosimetric quantities are tallied using ten sites instead of one to increase the scoring efficiency of the Monte Carlo simulation. (b) The absorbed dose and other dosimetric quantities are also tallied in annular regions located at various distances from the source.

* Although PENELOPE can transport electrons and positrons down to energies as low as 100 eV, the cross sections and physics below about 500 eV are more uncertain than those at higher energies because relevant refinements in the differential cross sections are neglected. Ongoing work by the PENELOPE team could have a positive affect on low energy, charged particle transport in the near future. Salvat, C. and Sempau, J. Personal communication. September 17, 2001.

gies below 100 eV and photons with energies less than 1 keV are assumed to deposit all of their energy locally.

Decay properties of tritium

Tritium (^3H) decays to ^3He , which is a stable element, through the beta decay process (half-life of $12.35 \text{ y}^{(24)}$) and, therefore, gives rise to a continuous spectrum of primary electron kinetic energies. For all Monte Carlo simulations, primary electron energies for ^3H were sampled from the normalised distribution function^(25–27) shown in Figure 2. The energy spectrum is sub-divided into 100 equal sized energy bins (bin width is 186 eV). The average energy of the first energy bin is 93.5 eV, which falls below the 100 eV electron transport cut-off energy used in PENELOPE. All beta particles sampled from the 93.5 eV energy bin are assumed to deposit all of their energy inside the tritide particle.

Tritide particle characteristics

All calculations reported in this work are based on the physical diameter of the tritide particle and not the aerodynamic or thermodynamic diameter typically used in particle inhalation models⁽¹⁰⁾. To obtain appropriate cross section data, the elemental composition and material density of the tritide particles are needed. The density of metal tritide particles is open to debate because their stoichiometry is both uncertain and variable*, and because the ^3H atoms are in the process of becoming ^3He atoms.

Some authors have used either the density of the metal or a handbook value for the density of a compara-

ble hydride. Densities of hydrides are available, or can be calculated from lattice constants or atom densities, for the five metals of interest here^(28–30). Except where explicitly noted otherwise, the elemental compositions and best-estimate material densities* listed in Table 1 were used for all Monte Carlo simulations. Hydride densities are scaled to minimum, maximum and best-estimate tritide densities using ratios of formula weights. The accuracy of these estimates depends on the assumption that the lattice constants of the resulting tritides are the same as those of the hydrides. The tritide particles are assumed to be embedded in an infinite medium of ICRU four-element soft tissue⁽¹⁴⁾ at a density of 1 g.cm^{-3} .

RESULTS**

Spectral emissions

In reading the literature, several previous studies have presented a quantity termed self-absorption fraction. By that term, previous authors meant the fraction of electrons (or energy) that was emitted from a metal tritide particle, not the fraction absorbed. For clarity, this paper uses the term emission fraction to mean the fraction of electrons emitted from the metal tritide particle and fraction of energy emitted to mean the fraction of ionising energy emitted from the radioactive transitions within a metal tritide particle that is carried away from the particle. That is, one minus the fraction of energy that is absorbed within the metal tritide particle.

Figure 3 shows a differential electron emission fraction [electrons per transition (i.e. per Bq.s) per keV] for

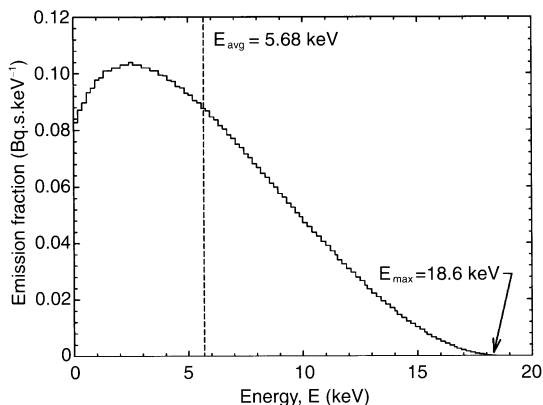


Figure 2. Tritium beta particle emission fraction^(19–21). For the PENELOPE Monte Carlo simulations, primary electron energies are sampled from a cumulative distribution function with 100 equal energy bins.

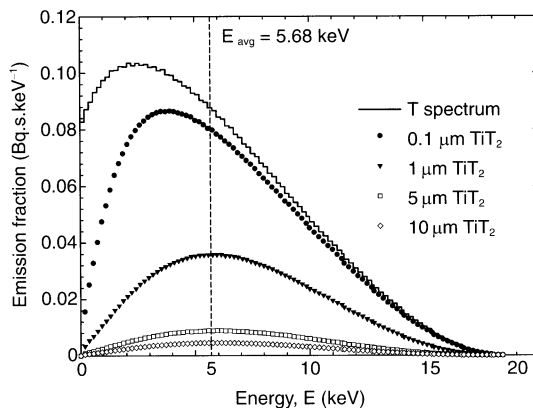


Figure 3. Electron emission fraction for TiT_2 particulates. Results shown are for 14.9 to 31.6 million tracks for each particle size.

* Gill, J. and Hafner, R. Personal communications. June 4, 2001.

** Supplemental information and data tables from the PENELOPE simulations are available on-line at <http://www.pnl.gov/eshs/pub/MetalTritide/>.

spherical ScT_2 particles of physical diameters 0.1, 1, 5, and 10 μm , as well as the sampled tritium spectrum (i.e. a particle diameter of 0). Two features are evident from this figure. First, the larger the particle, the smaller the fraction of electron radiation that escapes, a well-known result. Secondly, the emitted electron spectrum tends to 'harden' as the particle size increases, with average energy going from 5.68 keV (zero diameter point source) to 6.28 keV (0.1 μm), to 6.95 keV (1 μm), to 6.97 keV (10 μm). These average energies have an estimated standard error less than 0.1%, where the standard error is estimated as the difference between the average electron energy for two different Monte Carlo simulations using different random number sequences.

Figure 4 is a comparison of electron emission fractions for 0.1 μm diameter ScT_2 and HfT_2 particulates. The fraction of the electron radiation that escapes decreases with increasing particle density, and decreases with increasing atomic number. Furthermore, increasing the atomic number increases the spectrum hardening, as evidenced by the increasing modal value of each spec-

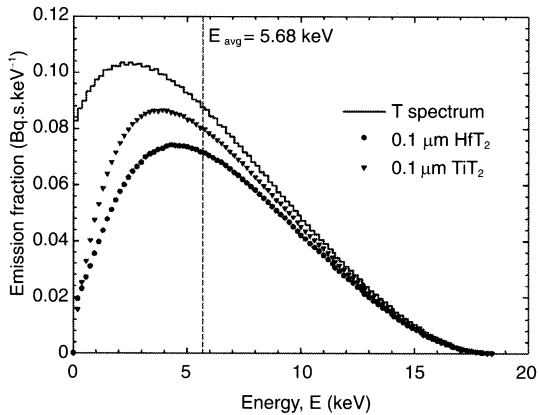


Figure 4. Comparison of electron emission fractions for TiT_2 and HfT_2 particulates. Results shown are 19.9 million tracks for TiT_2 and 20.4 million tracks for HfT_2 .

trum, with ScT_2 having an average electron energy of 6.28 keV, and HfT_2 having an average energy of 6.48 keV.

Figure 5 displays normalised electron and external bremsstrahlung photon emission spectra for 0.1 μm (a) and 5 μm (b) HfT_2 particles. Radionuclides undergoing beta decay also emit internal bremsstrahlung due to the sudden acceleration of the beta particle or electron (in electron capture)^(31–34), which is not treated here. Quite evident in Figure 5 is the expected result that the emitted bremsstrahlung spectrum is significantly softer (average photon energies of 3.08 keV and 4.70 keV, respectively, for the 0.1 and 5 μm particles) than the emitted electron spectrum (average electron energies of 6.48 keV and 7.00 keV, respectively). Photon emission above the 1.6 to 2.1 keV energy region is preferentially reduced because of the M-shell photoelectric absorption edge for Hf. Below these energies, the M-shell electrons are unavailable for X ray photon absorption, so the metal is somewhat more 'transparent' to photons at these lower energies. Emission of characteristic X rays and Auger electrons for the L and outer shells is neglected in the PENELOPE physics model.

Figure 6 shows the effect of atomic number on external bremsstrahlung photons emitted from surface of metal tritides. Bremsstrahlung, expressed as photons per transition (a), increases nearly linearly with particle size below 1 μm physical diameter. As the particle size increases, the beta particles experience a thicker target, giving an increased probability of a radiative interaction, yet the target is still not thick enough to absorb significantly the resultant photons. Bremsstrahlung also increases with atomic number for particle sizes below 1 μm .

For particle sizes up to 0.5 μm , bremsstrahlung production per transition, P_{brems} (photons/Bq.s), is approximately

$$P_{\text{brems}} (d \leq 0.5 \mu\text{m}) \propto d^{1.3} Z^{1.4}, \quad (1)$$

where d denotes physical diameter, and Z denotes the atomic number of the metal. As particle size increases

Table 1. Elemental compositions and densities of selected metal tritides. Hydride densities are scaled to minimum, maximum and best-estimate tritide densities using ratios of formula weights.

Metal tritide	Elemental composition	Metal density* (g.cm ⁻³)	Metal tritide density (g.cm ⁻³)		
			Estimated minimum	Estimated maximum	Best estimate
Scandium	ScT_2	2.99	2.99	3.21	3.10
Titanium	TiT_2	4.54	3.52	4.54	4.03
Zirconium	ZrT_2	6.51	5.15	6.51	5.83
Erbium	ErT_2	9.07	8.05	9.07	8.56
Hafnium	HfT_2	13.31	10.03	13.31	11.67

* From the PENELOPE cross section database [Sa99].

toward 1 μm , first Hf, then Zr, then Sc tritides show the curve turning downward, and finally decreasing, with the curves crossing so that the probability of external bremsstrahlung photons being emitted per transition is greatest for Sc at large particle sizes, and smallest for Hf. For particles 5 μm and larger, external bremsstrahlung is proportional to

$$P_{\text{brems}}(d \geq 5 \mu\text{m}) \propto d^{-0.8} Z^{-0.4}, \quad (2)$$

Panel (b) of Figure 6 shows bremsstrahlung photons expressed as photons per emitted electron. As particle size increases, two effects occur: there is a higher probability of producing external bremsstrahlung per transition, and a lower probability per transition of an

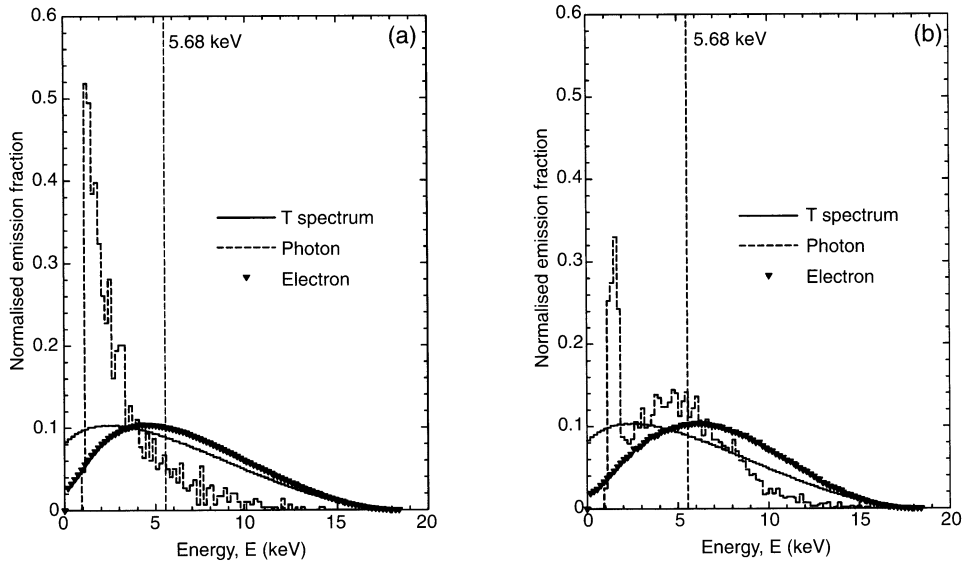


Figure 5. Normalised electron and photon emission spectra for HfT_2 . The area under the curve is unity for all emission spectra. (a) 0.1 μm HfT_2 (20.4 million tracks). (b) 5 μm HfT_2 (17.9 million tracks).

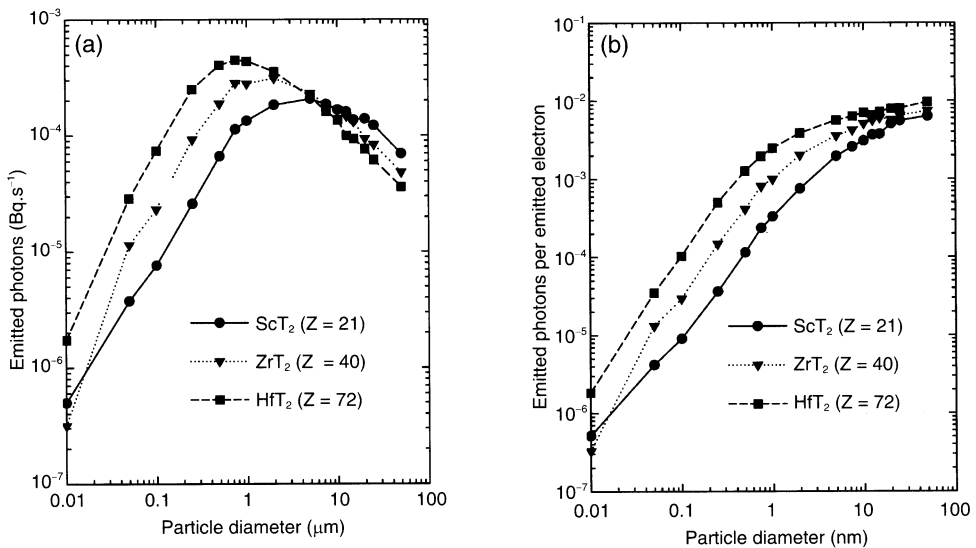


Figure 6. Photons emitted from the surfaces of selected tritides. Results for each tritide particle diameter are based on 3 to 4 million tracks for each particle size. (a) Photons emitted per transformation. (b) Number of photons emitted from the surface of a tritide per emitted electron.

electron emerging from the metal tritide particle. Thus the slopes for each of the three metal tritides are monotonically increasing functions of particle size, levelling out at about 10^{-2} photon per electron.

Emission fractions

This section presents characterisations of the effects of particulate diameter, composition, and density on the fraction of energy emitted. The dependence of energy emission fraction on metal tritide particle diameter and elemental composition on emission fractions for five metal tritides is shown in Figure 7. Also shown in Figure 7 is the energy emission fraction calculated from the formula in Kropf *et al*⁽⁷⁾, which overestimates the

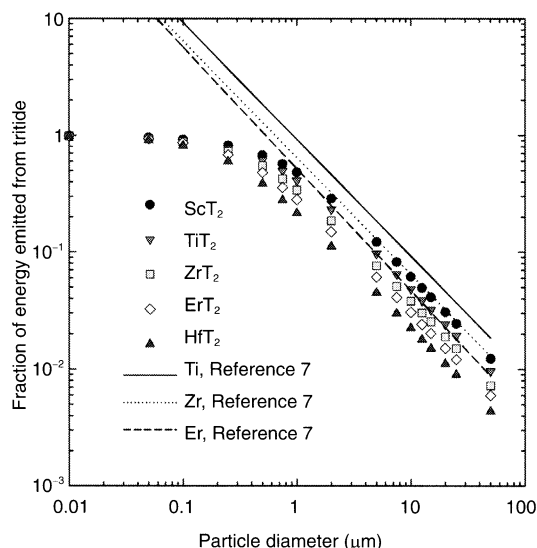


Figure 7. Energy emission fraction as a function of particle size. Results for each tritide particle diameter are based on 3 to 4 million tracks. The estimated standard deviation associated with the emission fraction is less than 1 to 2% for all particle sizes.

Table 2. Effects of tritide composition on the energy emission fraction. Results for each tritide particle diameter are based on approximately 4 million tracks. The estimated standard deviation associated with the emission fraction is less than 1 or 2% for all particle sizes. The metals Sc and Hf represent the respective tritides with vanishingly small amounts of tritium.

Diameter (μm)	Fraction of energy emitted from tritide				Ratio of emission fractions	
	Sc	ScT ₂	Hf	HfT ₂	Sc:ScT ₂	Hf:HfT ₂
0.01	0.9934	0.9922	0.9817	0.9805	1.0012	1.0011
0.10	0.9301	0.9208	0.7972	0.7899	1.0101	1.0092
1.00	0.5162	0.4827	0.1976	0.1916	1.0685	1.0325
5.00	0.1361	0.1219	0.0405	0.0393	1.1194	1.0337
10.00	0.0688	0.0614	0.0205	0.0197	1.1246	1.0341

amount of energy emitted from the tritide particulate. Dose estimates based on the Kropf *et al* formula are too high by at least a factor of 2 or 3, and that formula has non-physical behaviour (i.e. exceeds 1) for particle diameters less than about $1\ \mu\text{m}$.

Because of lack of knowledge of tritide stoichiometry, and because of its variability, it is important to explore the effects of tritide stoichiometry on the energy emission fraction (Table 2). The composition of the particle affects the emitted energy fraction by less than 3% for Hf and less than 8% for Sc. Table 2 shows that uncertainties associated with tritide stoichiometry increase as the atomic number decreases.

The effects of material density on the energy emission fraction are shown in Tables 3 to 7 for Sc, Ti, Zr, Er, and Hf tritides, respectively. Tables 3 to 7 are based on the ranges of densities given in Table 1. The variations in energy emission fraction are roughly a linear function of density for large particles, with a slope of -1 . Density effects increase as particle size increases.

Radial dose distribution

Figure 8 shows the radial dose distribution outside representative HfT₂ particles. The absorbed dose is approximately constant within the interior of the particle. The radial dose distribution outside the particle decreases in a bi-exponential manner with distance away from the surface of the tritide particle. The overall pattern of the radial dose distribution is quite similar for other particle types and sizes (data not shown). The continuous slowing down approximation (CSDA) range of an 18.6 keV electron (the maximum-energy electron emitted by tritium) in soft tissue is $7.63\ \mu\text{m}$ ⁽³⁵⁾. For distances less than about $7\ \mu\text{m}$, absorbed dose is mainly determined by the electron component of the radiation field.

For distances greater than $7\ \mu\text{m}$, these calculations show that the absorbed dose is due to bremsstrahlung. For distances in the range of 7 to $100\ \mu\text{m}$ from the centre of $10\ \mu\text{m}$ HfT₂ particles (not shown), the absorbed dose per transition drops approximately as the

–2.8 power of the distance from the centre of the particle. For distances in the range of 8 to 100 μm from the centre of 1 μm HfT_2 particles, the absorbed dose drops approximately as the –3.0 power of the distance

from the surface of the particle. One would expect such values because of geometry (inverse-square law) and attenuation (absorption and beam hardening with increasing penetration). The faster decrease with smaller

Table 3. Effects of material density on the energy emission fraction for ScT_2 . Results for each tritide particle diameter are based on approximately 5 million tracks each particle size. The estimated standard deviation associated with the emission fraction is less than 1% for all particle sizes.

Diameter (μm)	Fraction of energy emitted from Sc tritide			
	Minimum	Best estimate	Maximum	% Difference (Max.–Min.)
0.01	0.9920	0.9922	0.9925	0.06
0.10	0.9181	0.9208	0.9234	0.58
1.00	0.4726	0.4827	0.4936	4.35
5.00	0.1181	0.1219	0.1265	6.88
10.00	0.0593	0.0614	0.0635	6.94
Density (g.cm^{-3})	3.211	3.100	2.989	7.16

Table 4. Effects of material density on the energy emission fraction for TiT_2 . Results for each tritide particle diameter are based on approximately 5 million tracks each particle size. The estimated standard deviation associated with the emission fraction is less than 2% for all particle sizes.

Diameter (μm)	Fraction of energy emitted from Ti tritide			
	Minimum	Best estimate	Maximum	% Difference (Max.–Min.)
0.01	0.9890	0.9903	0.9915	0.25
0.10	0.8894	0.9010	0.9127	2.59
1.00	0.3771	0.4106	0.4499	17.73
5.00	0.0858	0.0962	0.1098	24.91
10.00	0.0429	0.0482	0.0552	25.48
Density (g.cm^{-3})	4.540	4.030	3.520	25.31

Table 5. Effects of material density on the energy emission fraction for ZrT_2 . Results for each tritide particle diameter are based on approximately 5 million tracks each particle size. The estimated standard deviation associated with the emission fraction is less than 1.5% for all particle sizes.

Diameter (μm)	Fraction of energy emitted from Zr tritide			
	Minimum	Best estimate	Maximum	% Difference (Max.–Min.)
0.01	0.9878	0.9891	0.9904	
0.10	0.8697	0.8825	0.8956	2.93
1.00	0.3124	0.3411	0.3754	18.49
5.00	0.0682	0.0759	0.0855	22.80
10.00	0.0340	0.0380	0.0430	23.77
Density (g.cm^{-3})	6.506	5.830	5.154	23.19

particles is comprehensible because the bremsstrahlung spectrum is 'softer'.

Because inhaled metal tritides may be engulfed by a macrophage or surrounded by insensitive biomaterials

(e.g. mucous), bremsstrahlung may be the only biologically relevant radiation emitted by metal tritides.

Microdosimetry

Figure 9 shows the specific energy, single-event distribution⁽³⁶⁾ for a 1 μm diameter region of tissue located at various radial distances r from the centre of a 100 nm HfT₂ particulate (refer to Figure 1). For tally sites located farther away from the surface of the tritide, the single-event spectrum shifts towards larger specific energy events. The frequency-mean specific energy per event increases 16.4% from 0.663 to 0.772 Gy as the radial distance of the site from the centre of the tritide increases from 0.5 μm to 3.5 μm. Specific energies of 2.17 and 2.52 keV and lineal energies of 3.25 keV.μm⁻¹ and 3.78 keV.μm⁻¹, respectively. The probability the tally site is 'hit' by radiation escaping from the tritide decreases from 0.24 to 2.36×10⁻⁴ because of absorption by the tissue surrounding the tritide and because of geometric (1/r²) attenuation.

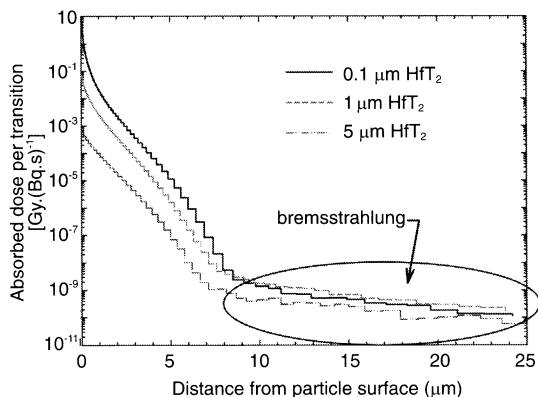


Figure 8. Radial distribution of absorbed dose.

Table 6. Effects of material density on the energy emission fraction for ErT₂. Results for each tritide particle diameter are based on approximately 5 million tracks each particle size. The estimated standard deviation associated with the emission fraction is less than 1.5% for all particle sizes.

Diameter (μm)	Fraction of energy emitted from Er tritide			
	Minimum	Best estimate	Maximum	% Difference (Max.-Min.)
0.01	0.9866	0.9878	0.9882	0.16
0.10	0.8499	0.8606	0.8660	1.86
1.00	0.2648	0.2820	0.2926	9.87
5.00	0.0564	0.0606	0.0634	11.53
10.00	0.0282	0.0304	0.0317	11.55
Density (g.cm ⁻³)	9.070	8.560	8.054	11.87

Table 7. Effects of material density on the energy emission fraction for HfT₂. Results for each tritide particle diameter are based on approximately 5 million tracks each particle size. The estimated standard deviation associated with the emission fraction is less than 2.3% for all particle sizes.

Diameter (μm)	Fraction of energy emitted from Hf tritide			
	Minimum	Best estimate	Maximum	% Difference (Max.-Min.)
0.01	0.9805	0.9831	0.9856	0.51
0.10	0.7899	0.8137	0.8384	5.96
1.00	0.1912	0.2153	0.2466	25.71
5.00	0.0394	0.0451	0.0521	28.23
10.00	0.0196	0.0223	0.0259	28.04
Density (g.cm ⁻³)	13.310	11.670	10.030	28.11

Figure 10 shows the single-event distribution for a 5 μm diameter region of tissue located at the surface of the 0.1 and 5 μm tritides of Sc and Hf. A 5 μm diameter site encloses approximately the same volume as a typical mammalian cell nucleus. For the smaller 100 nm tritides, the shape of the single-event distribution shifts towards slightly larger specific energies. The single-event distributions are not statistically different for the 5 μm Sc and Hf tritides. As the particle size increases, the shape of the single-event distribution shifts towards larger specific energy events. For example, the frequency-mean specific energy increases by 21.6% from 11.3 to 13.7 mGy as the diameter of a HfT₂ increases from 0.1 to 5 μm. The frequency-mean lineal energy increases from 1.38 keV.μm⁻¹ to 1.68 keV.μm⁻¹. Such lineal energies are characteristic of low-linear energy transfer (low-LET) radiation.

Apparent activity and observed activity

The medical physics community uses the concept of apparent activity⁽³⁷⁾ to express quantitatively the fact that some emissions from brachytherapy sources are absorbed by the source or its encapsulation. Apparent activity is based on dose: it is that unshielded and unself-absorbed activity that would produce the same dose as the source in question. Internal dosimetrists at the US Department of Energy’s (DOE’s) Mound Laboratory have introduced a subtly different concept they call observed activity⁽³⁸⁾. Observed activity is that activity of tritium that would produce the same count rate in a liquid scintillation counter as the particle being measured.

The electron spectrum emitted from a metal tritide particle is ‘harder’, that is, it has a higher average energy, than the beta spectrum of pure tritium. For example, the average electron energy emitted from

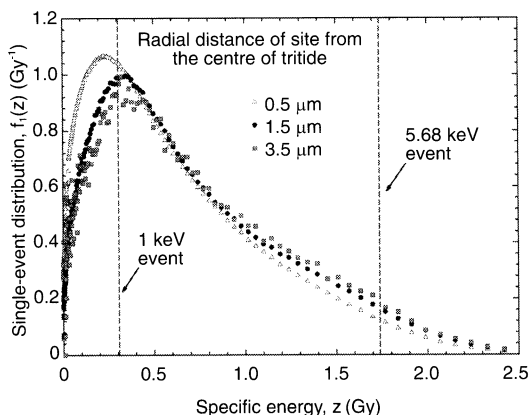


Figure 9. Single-event distribution for a 1 μm diameter region of tissue located near the surface of a 100 nm HfT₂ particulate. Results shown are for 20.4 million tracks. The tally site has a mean chord length of 0.667 μm.

5 μm particles of HfT₂ is 7.00 keV, compared with 5.68 keV for pure T. These electrons would produce 1.23 (= 7.00/5.68) times the dose that a similar number of beta particles from pure tritium would produce. This is termed the average electron energy ratio, R_{acee},

$$R_{acee} = \frac{\bar{E}_{MT_2}}{\bar{E}_T} \tag{3}$$

where \bar{E}_{MT_2} is the average electron energy emitted by the metal tritide and \bar{E}_T is the average electron energy by tritium.

One would expect that the more penetrating electrons from a metal tritide particle would be more efficiently detected by a liquid scintillation counter than the beta particles emitted from pure tritium. One would also expect that a liquid scintillation detector’s efficiency for electrons emitted from metal tritide particles could be related to its efficiency for pure tritium. Making the assumption that a liquid scintillation counter detects every particle above a particular cut-off energy, it is possible to determine the metal tritide electron counting efficiency as a function of the beta counting efficiency, as shown in Figure 11 for 5 μm particles of HfT₂. Using cdf to denote the cumulative probability density function of the normalised emission energy spectrum, Figure 11 shows [1 - cdf(HfT₂)], the fraction of electrons occurring above a given energy, plotted as a function of [1 - cdf(T)], the fraction of tritium beta particles occurring above the same energy.

Figure 11 shows, for example, a nominal 67% counting efficiency for pure tritium (which occurs at a counting threshold of 3.25 keV) gives an electron counting efficiency of 84%. The ratio of these two efficiencies,

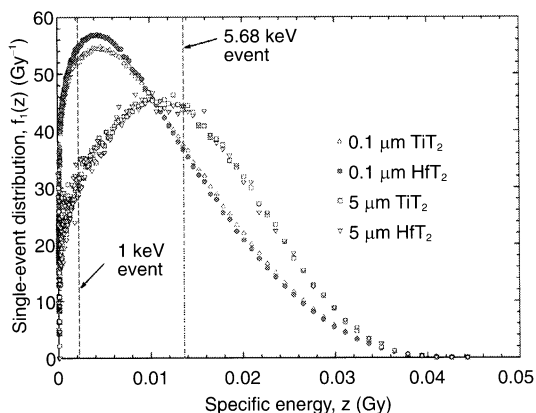


Figure 10. Single-event distribution for 5 μm diameter region of tissue located near the surface of selected Ti and Hf tritide particulates. The centre of the tally site positioned so that the edges of the metal tritide and tally site are touching (r = 2.55 or 5.0 μm in Figure 1). The tally site has a mean chord length of 3.33 μm.

$$R_{\text{eff}} = \frac{1 - \text{cdf}(\text{HfT}_2)}{1 - \text{cdf}(\text{T})} \quad (4)$$

is shown in Figure 12 for counting thresholds up to 16 keV. The apparent activity (i.e. for equal dose) is related to the observed activity (equal counts) by

$$A_{\text{app}} = A_{\text{obs}} \frac{R_{\text{acc}}}{R_{\text{eff}}} \quad (5)$$

For the example of 5 μm particles of HfT_2 , $A_{\text{app}} = (1.23/1.25) A_{\text{obs}} = 0.98 A_{\text{obs}}$. This correction is unlikely to be significant and can be ignored for practical purposes.

CONCLUSIONS

All of the results reported are based on Monte Carlo simulations. The data and analyses presented in this report provide new, more detailed information on the dosimetry of five different metallic tritides with a variety of physical diameters and each with a range of densities. The absorbed dose calculations presented here are likely to be more accurate than those previously published and include data for additional metal tritides of interest to the DOE. However, as many factors (e.g. uncertainties in cross section data used in the Monte Carlo simulations) have the potential to affect the reported results, a comparison of measured and calculated emission spectra, as well as other dosimetric quantities, would be welcome.

The fraction of beta kinetic energy that is emitted from a particle is shown to decrease with increasing particle diameter, increasing metal atomic number, and increasing density. This fraction is called self-absorption factor by other authors.

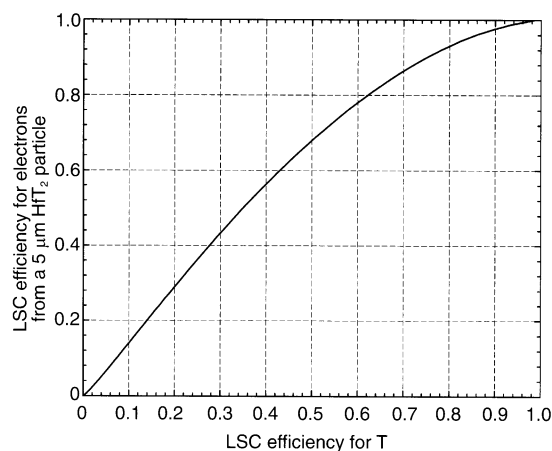


Figure 11. Liquid scintillation counting (LSC) efficiency for 5 μm HfT_2 plotted against the LSC for tritium. The LSC is calculated based on the assumption that all electrons above a fixed cut-off energy are detected in the scintillation counter.

Electron radiation interacting with the metal tritide particles produces external bremsstrahlung, which is shown to be of lower average energy than the electron radiation. Just outside the surface of a tritide particle, the dose from external bremsstrahlung radiation is many orders of magnitude smaller than the dose from the electrons. However, at distances greater than about 5 to 8 μm from the surface of a particle, almost all of the dose is due to the bremsstrahlung radiation. The fraction of energy emitted as bremsstrahlung varies with both metal and particle diameter, approaching 1% of the energy emitted as electron radiation for particles larger than 10 μm in diameter. When metal tritide particles are inhaled, they may be deposited at various points in the respiratory tract. If the tritide particle undergoes phagocytosis by a macrophage or surrounded by insensitive biomaterials (e.g. mucous), energy deposited 5 to 8 μm away from the metal tritide may be the only biologically significant dose.

Microdosimetric event-size spectra are presented for selected tritide particles; no data were previously available in the literature on the microdosimetric properties of metal tritides. Radiation emitted by tritide particles can be characterised as low-LET radiation.

The spectral properties of the electron radiation escaping from the metal tritides show that analysis of liquid scintillation measurements in terms of 'observed activity' is likely to be more than adequate for dosimetric purposes.

Future work should include investigations of the contributions of internal bremsstrahlung, the bremsstrahlung emitted from the nucleus during beta decay⁽³¹⁻³⁴⁾. Studies to better quantify the uncertainties associated with (1) the density and composition of the particulate, (2) the uniformity of tritium deposition within the particulate, (3) electron and photon cross sections, especially for electron energies less than 1 keV, (4)

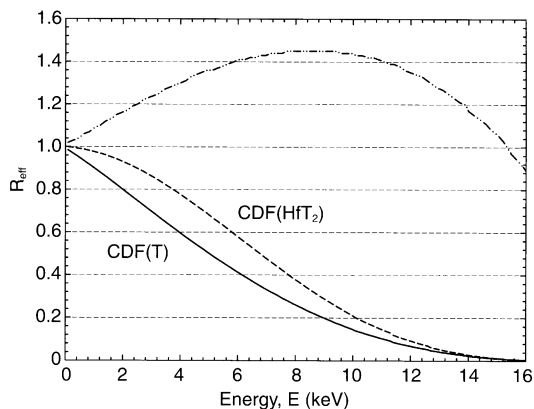


Figure 12. R_{eff} (---) is the ratio of counting efficiency for the tritide particle to the counting efficiency for pure T given by Equation 4.

source–energy spectrum, and (5) the shape of the particulates would also be useful.

Rabovsky, and R. J. Traub for guidance on the properties of metal tritide particulates as well as many useful comments and suggestions on the manuscript. Pacific Northwest National Laboratory is operated for the US Department of Energy by Battelle Memorial Institute under Contract DE-AC06-76RLO-1830. This work was supported by the DOE Office of Worker Protection Programs.

ACKNOWLEDGEMENTS

The authors thank Drs J. Gill, J. R. Johnson, R. Hafner, M. Sharfi, I. Kawrakow, J. K. Shultis, J. L.

REFERENCES

1. International Commission on Radiological Protection. *Limits for Intakes of Radionuclides by Workers*. ICRP Publication No 30, Part 1, Ann. ICRP **2**(3/4) (Oxford: Pergamon Press) (1979).
2. International Commission on Radiological Protection. *Age-Dependent Doses to Members of the Public from Intake of Radionuclides: Part 1*. ICRP Publication No 56, Ann. ICRP **20**(2) (Oxford: Pergamon Press) (1989).
3. International Commission on Radiological Protection. *Age-Dependent Doses to Members of the Public from Intake of Radionuclides: Part 2 Ingestion Dose Coefficients*. ICRP Publication No 67, Ann. ICRP **23**(3/4) (Oxford: Pergamon Press) (1993).
4. International Commission on Radiological Protection. *Age-Dependent Doses to Members of the Public from Intake of Radionuclides: Part 4 Inhalation Dose Coefficients*. ICRP Publication No 71, Ann. ICRP **25**(3–4) (Oxford: Pergamon Press) (1995).
5. International Commission on Radiological Protection. *Age-Dependent Doses to Members of the Public from Intake of Radionuclides: Part 5 Compilation of Ingestion and Inhalation Dose Coefficients*. ICRP Publication No 72, Ann. ICRP **26**(1) (Oxford: Pergamon Press) (1996).
6. Cheng, Y. S., Dahl, A. R. and Jow, H. N. *Dissolution of Metal Tritides in a Simulated Lung Fluid*. Health Phys. **73**(4), 633–638 (1997).
7. Kropf, R. F., Wang, Y. and Cheng, Y. S. *Self-absorption of Tritium Betas in Metal Tritide Particles*. Health Phys. **75**(4), 398–404 (1998).
8. Inkret, W. C., Schillaci, M. E., Boyce, M. K., Cheng, Y. S., Efurud, D. W., Little, T. T., Miller, G., Musgrave, J. A. and Wermer, J. R. *Internal Dosimetry for Inhalation of Hafnium Tritide Aerosols*. Radiat. Prot. Dosim. **93**(1), 55–60 (2001).
9. Richardson, R. B. and Hong, A. *Dose to Lung from Inhaled Tritiated Particles*. Health Phys. **81**(3), 313–324 (2001).
10. International Commission on Radiological Protection. *Human Respiratory Tract Model for Radiological Protection*. ICRP Publication No 66, Ann. ICRP **24**(1–3) (Oxford: Pergamon Press) (1994).
11. Briesmeister, J. F. *MCNPTM — A General Monte Carlo N-Particle Transport Code, Version 4B*. LA-12625-M, Version 4B (Los Alamos, New Mexico: Los Alamos National Laboratory) (1997).
12. Nelson, W. R., Hirayama, H. and Rogers, D. W. O. *The EGS4 Code System*. SLAC-265 (Available at <http://www.slac.stanford.edu/pubs/slacreports/slac-r-265.html>) (Palo Alto, California: Stanford Linear Accelerator Center) (1985).
13. Baró, J., Fernández-Varea, J. M., Sempau, J. and Salvat, F. *PENELOPE: An Algorithm for Monte Carlo Simulation of the Penetration and Energy Loss of Electrons and Positrons in Matter*. Nucl. Instrum. Methods **B100**, 31–46 (1995).
14. Salvat, F., Fernández-Varea, J. M., Baró, J. and Sempau, J. *PENELOPE Code System to Simulate Coupled Electron Gamma-Ray Transport at High Energies*. Code Package CCC-682 (Oak Ridge, Tennessee: Radiation Safety Information Computational Center (RSICC)). (1999).
15. Sempau, J., Acosta, E., Baró, J., Fernández-Varea, J. M. and Salvat, F. *An algorithm for Monte Carlo Simulation of Coupled Electron–Photon Transport*. Nucl. Instrum. Methods **B132**, 377–390 (1997).
16. Berger, M. J. and Wang, R. *Multiple-scattering Angular Deflections and Energy-loss Straggling*. In: Monte Carlo Transport of Electrons and Photons. Eds. T. M. Jenkins, W. R. Nelson, and A. Rindi (New York: Plenum) pp. 21–56 (1988).
17. Seltzer, S. M. *An Overview of ETRAN Monte Carlo Methods*. In: Monte Carlo Transport of Electrons and Photons. Eds. T. M. Jenkins, W. R. Nelson and A. Rindi (New York: Plenum) pp. 153–181 (1988).
18. Halbleib, J. A., Kensek, R. P., Mehlhorn, T. A., Valdez, G. D., Seltzer, S. M. and Berger, M. J. *ITS Version 3.0: The Integrated TIGER Series of Coupled Electron/Photon Monte Carlo Transport Codes*. Code Package CCC-467 (Oak Ridge, Tennessee: Radiation Safety Information Computational Center (RSICC)) (1992).
19. Turner, J. E., Magee, J. L., Wright, H. A., Chatterjee, A., Hamm, R. N. and Ritchie, R. H. *Physical and Chemical Development of Electron Tracks in Liquid Water*. Radiat. Res. **96**, 437–449 (1983).
20. Turner, J. E., Hamm, R. N., Wright, H. A., Ritchie, R. H., Magee, J. L., Chatterjee, A. and Bolch, W. E. *Studies to Link the Basic Radiation Physics and Chemistry of Liquid Water*. Radiat. Phys. Chem. **32**, 503–510 (1988).
21. Wilson, W. E., Miller, J. H. and Nikjoo, H. *PITS: A Code Set for Positive Ion Track Structure*. In: Computational Approaches in Molecular Radiation Biology. Eds M. N. Varma and A. Chatterjee (New York: Plenum Press) (1994).
22. Wilson, W. E. and Nikjoo, H. *A Monte Carlo Code for Positive Ion Track Simulation*. Radiat. Environ. Biophys. **38**, 97–104 (1999).

23. Stewart, R. D., Wilson, W. E., McDonald, J. C. and Strom, D. J. *Microdosimetric Properties of Ionizing Electrons in Water: A Test of the PENELOPE Code System*. Phys. Med. Biol. **47**(1), 77–88 (2002).
24. International Commission on Radiological Protection. *Radionuclide Transformations: Energy and Intensity of Emissions*. ICRP Publication No 38, Ann. ICRP **11–13** (Oxford: Pergamon Press) (1983).
25. Eckerman, K. F., Westfall, R. J., Ryman, J. C. and Cristy, M. *Nuclear Decay Data Files of the Dosimetry Research Group*. ORNL/TM-12350 (Oak Ridge, Tennessee: Oak Ridge National Laboratory) (1993).
26. Eckerman, K. F., Westfall, R. J., Ryman, J. C. and Cristy, M. *Availability of Nuclear Decay Data in Electronic Form, Including Beta Spectra not Previously Published*. Health Phys. **67**(4), 338–345 (1994).
27. Eckerman, K. F. *NUDECAY: Nuclear Decay Data for Radiation Dosimetry Calculations for ICRP and MIRD*. Data Library DLC-172 (Oak Ridge, Tennessee: Radiation Safety Information Computational Center (RSICC)) (1995).
28. Libowitz, G. G. *The Solid State Chemistry of Binary Metal Hydrides* (New York: W. A. Benjamin) (1965).
29. Mueller, W. M., Blackledge, J. P. and Libowitz, G. G. *Metal Hydrides* (New York: Academic Press) (1968).
30. Winter, M. *WebElements*. [http://www. WebElements.com](http://www.WebElements.com) (University of Sheffield, UK) (2001).
31. Knipp, J. A. and Uhlenbeck, G. E. *Emission of Gamma Radiation During the Beta Decay of Nuclei*. Physica **III**(6), 425–439 (1936).
32. Bloch, F. *On the Continuous γ -Radiation Accompanying the β -Decay*. Phys. Rev. **50**, 272–278 (1936).
33. Wang Chang, C. S. and Falkoff, D. L. *On the Continuous Gamma-radiation Accompanying the Beta-Decay of Nuclei*. Phys. Rev. **76**(3), 365–371 (1949).
34. Budick, B., Chen, J. and Lin, H. *Bremsstrahlung from Tritium β Decay*. Phys. Rev. C **46**(4), 1267–1275 (1992).
35. Berger, M. J., Coursey, J. S. and Zucker, M. A. *Stopping-Power and Range Tables for Electrons, Protons, and Helium Ions*. <http://physics.nist.gov/PhysRefData/Star/Text/contents.html> (Gaithersburg, Maryland: National Institute of Standards and Technology) (2000).
36. International Commission on Radiation Units and Measurements. *Microdosimetry*. ICRU Report No 36 (Bethesda, Maryland: ICRU Publications) (1983).
37. Nath, R., Anderson, L. L., Luxton, G., Weaver, K. A., Williamson, J. F. and Meigooni, A. S. *Dosimetry of Interstitial Brachytherapy Sources: Recommendations of the AAPM Radiation Therapy Committee Task Group No. 43. American Association of Physicists in Medicine*. Med. Phys. **22**(2), 209–234 (1995).
38. Miamisburg Environmental Management Project. *Mound Technical Basis Document for Stable Tritiated Particulate and Organically Bound Tritium*. MD-10516 Issue 2 (Miamisburg, Ohio: BWXT, Inc) (2000).